PHOTODETECTORS QUANTUM WELL

A conventional photodetector operates by generating carriers which are produced by the absorption of a photon across the bandgap, E_g, of the active semiconducting region. This absorption excites an electron from the valence band to the conduction band (see Fig. 1), thereby producing a photocurrent. However, in order for this absorption to occur, the photon energy $h\nu$ must be larger than the bandgap. This limits the useful spectral range of these detectors to the ultraviolet through near infrared region (optical wavelength $\lambda = 0.3–5\ \mu$m). Longer wavelengths (e.g., $\lambda = 8–12\ \mu$m which is an important atmospheric spectral window) require materials of very low bandgap (e.g., $Hg_{1-x}Cd_xTe$) that are difficult to grow, process, and fabricate into useful devices (1). Thus, it is especially difficult to make large area uniform arrays of such semiconductors, which are essential for infrared imaging applications (2). The other approach to making long wavelength arrays relies on Schottky barrier detectors which have low quantum efficiency and also require much lower operating temperatures (3).

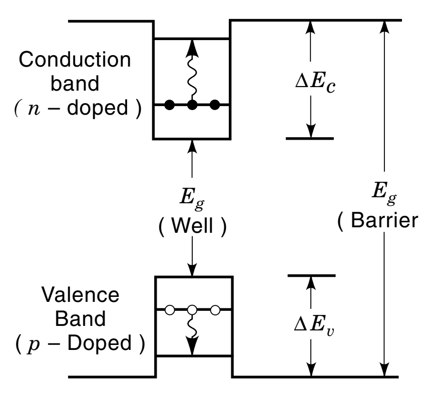

Figure 1. Band structure of quantum well. Intersubband absorption between conduction band electrons levels E_1 and E_2, or valence band hole levels H_1 and H_2 are shown.

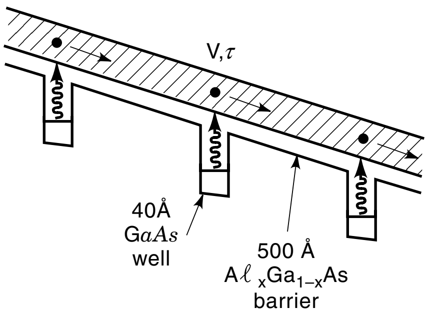

Figure 2. Conduction band structure for a bound to contuum QWIP, showing the photoexcitation and electron transport process.

For these reasons a new type of photodector (4) has been developed based on the absorption of carriers within the same band (i.e. intersubband absorption) (5). This allows the use of large bandgap materials which are much easier to grow and fabricate into devices, and are also far more uniform in properties than low bandgap materials. In order to use such large gap semiconductors, a *sandwich* of two different bandgap materials is grown on a substrate (using for example molecular beam epitaxy). This creates a quantum well of the lower gap material surrounded by the larger gap barrier material, as shown in Fig. 1. Such a quantum well will have several energy levels determined by the width of the well, L, and the difference in the bandgaps ΔE_g of the two semiconductor materials. By controlling both of these parameters the energy separation of the two lowest intersubband levels $\Delta E = E_2 - E_1$ can be varied over a wide range of values corresponding of absorption at wavelengths of $\lambda = 3$–$20\ \mu$m. In order to create infrared optical absorption, carriers are placed in the lowest energy level E_1 by doping the well. Such a doped quantum well will have a strong optical absorption peak at an energy corresponding to ΔE. Thus, by collecting the carriers which are photoexcited out of the well and into the conduction band where they are transported, a photocurrent is generated. This new type of device is called a quantum well infrared photodetector (QWIP) (6). In order to increase the absorption strength, a periodic stack of many quantum wells, N (typically 50 periods of 40–60-Å width), are used as shown in Fig. 2.

THEORY

The most common semiconductor used for growing these wells is GaAs with $Al_xGa_{1-x}As$ barriers since these materials are lattice matched, easy to grow, and by varying the Al composition the barrier height ΔE_g can be readily changed. One important feature of the intersubband absorption is that due to quantum mechanical selection rules, the optical electric field must be perpendicular to the wells (5) (i.e. along the growth direction). For quick measurements, the sample is polished at an angle (e.g. 45°), and the radiation is incident on this face as shown in Fig. 3, giving a substantial electric field component in the normal direction. For large imaging arrays, optical gratings (7) (either periodic or random) are used to efficiently couple the light as shown in Fig. 4.

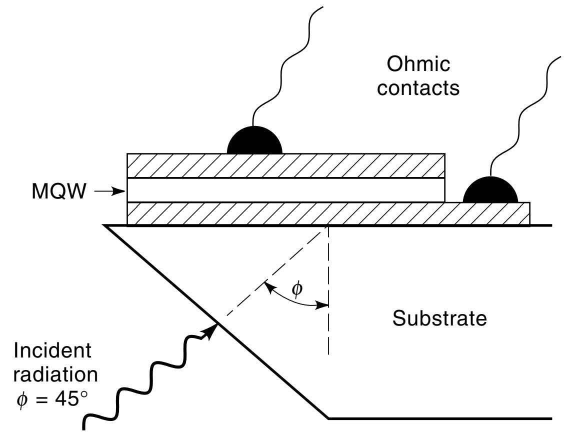

Figure 3. Geometry for QWIP photoresponse measurement.

QWIP PERFORMANCE

Responsivity and Dark Current

The responsivity R of the QWIP (i.e. how much current is generated by each incident photon) is given by (6)

$$R = (e/\hbar\nu)\eta_a p_e g \tag{1}$$

where e is the electronic charge, η_a is the absorption quantum efficiency, p_e is the carrier escape probability out of the well, and g is the optical gain (which is equal to the carrier lifetime/transit time). The responsivity as a function of wavelength is shown for several $GaAs/Al_xGa_{1-x}As$ QWIPs having varying well widths and depths in Fig. 5, illustrating the ability to vary the peak response over a wide range. In addition to the responsivity, R, the detector sensitivity (i.e. the signal-to-noise ratio) also depends on the dark current I_d (i.e. the current without light). This is shown for a QWIP having a peak response at $\lambda = 8.4\ \mu$m in Fig. 6. Note that I_d depends strongly on temperature, T, decreasing approximately exponentially with decreasing T due to the reduced thermal excitation of carriers out of the well.

In order to optimize the QWIP performance, it is important to maximize R, minimize I_d, and control contact effects (8). These parameters depend strongly on the position of the lowest excited state, E_2, in the well. If E_2 is above the top of the quantum well barrier (as in the insert in Fig. 7), carriers optically excited to this continuum state will be efficiently collected and therefore the responsivity will be high. However, thermally generated carriers will also be easily collected and this I_d will be large. On the other hand if E_2 is bound in the

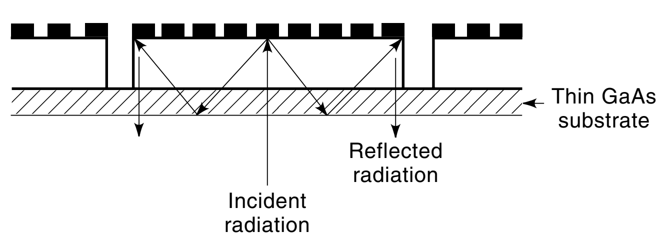

Figure 4. Structure of a QWIP having a grating etched into the top surface of the pixels.

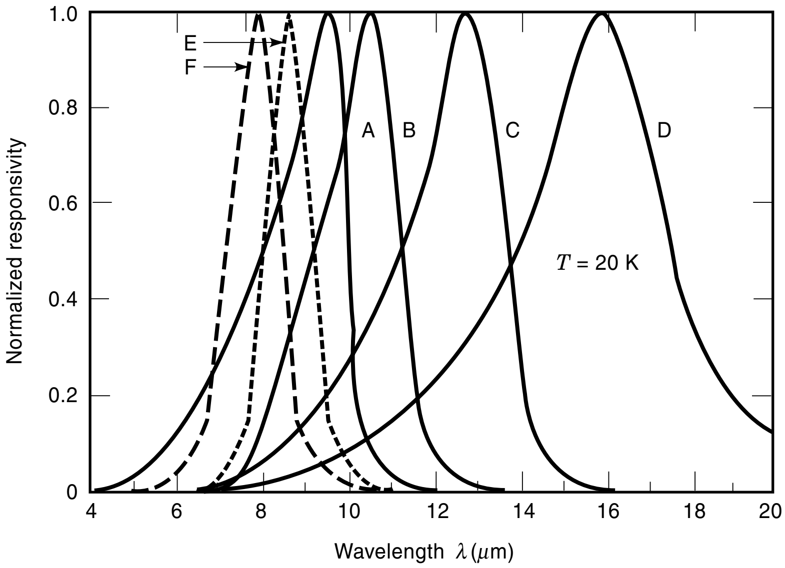

Figure 5. Normalized QWIP responsivity, showing the ability to easily vary the spectral response by changing the quantum well parameters. The barrier width is $L_b = 500$ Å, while the quantum well width L_w and the Al content x in $Al_xGa_{1-x}As$ are given for the various samples by: A (40 Å, 0.26); B (40 Å, 0.25); C (60 Å, 0.15); D (70 Å, 0.10); E (50 Å, 0.26); and F (50 Å, 0.30/0.26). (See inserts on Figures 7–9.)

well (i.e. below the top of the barrier) as indicated in the lower insert in Fig. 8, then the opposite is true: i.e. both R and I_d are low at low voltage. The intermediate situation where the excited state is exactly resonant at the top of the well or the quasi-continuum case indicated in the top insert in Fig. 8 (where there are thin tunneling barriers near the top of the well) is near optimum, yielding a large responsivity and a low dark current (9).

The reason that the dark current decreases the sensitivity is that it generates current noise (given for low quantum well capture probability, p_c) as (6,10),

$$i_n = (4eI_T g \, \Delta f)^{1/2} \tag{2}$$

where Δf is the bandwidth of the signal, and where $I_T = I_d + I_p$ is the total current consisting of both the dark and photocurrents. In fact, by using this current noise relation the optical gain g can be determined from measurements of the noise, and then p_c can be determined by the approximate relation (6,10), (valid for small p_c) $p_c \approx (1/g\ N)$, where N is the number of wells in the QWIP. Figure 9 shows that the measured capture probability decreases strongly as a function of bias. In contrast to this the escape probability and hence the net quantum efficiency $\eta = \eta_a p_e$ increase strongly with bias as shown in Figs. 10 and 11.

High Speed Response

Because of the very short intersubband lifetimes (1–10 ps), as well as the rapid transport of the photoexcited carriers, the intrinsic QWIP response speed is exceptionally fast. Heterodyne QWIP detectors have demonstrated bandwidths in excess of 82 GHz (11), which makes them ideally suited for a

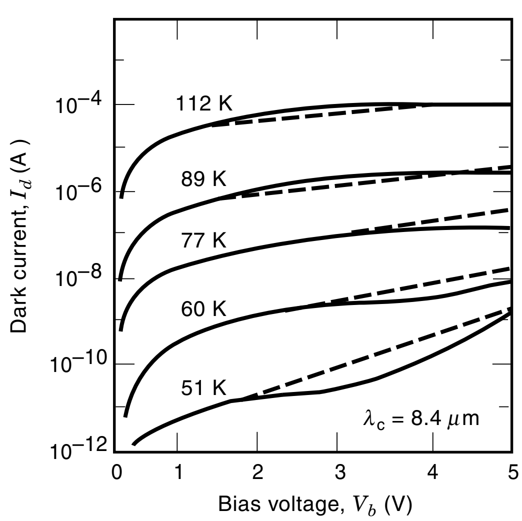

Figure 6. Comparison of experimental (solid curves) and theoretical (dashed) QWIP dark current curves at various temperatures.

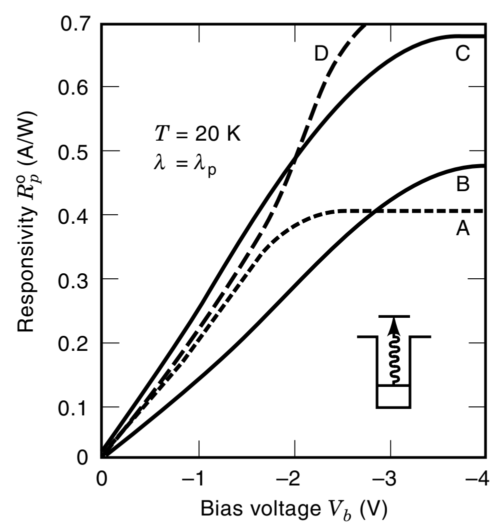

Figure 7. Bias-dependent (bound to continuum) QWIP responsivities for samples A–D of Fig. 4. The insert shows the conduction band diagram.

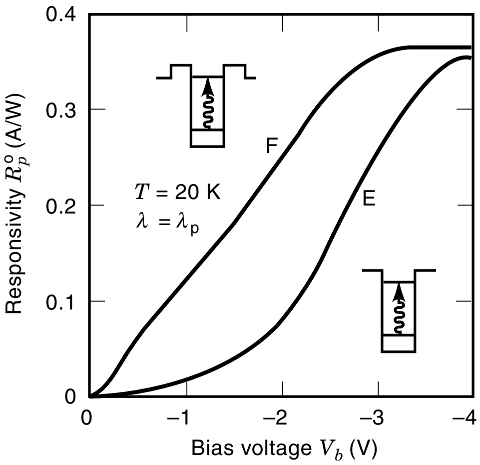

Figure 8. Bias-dependent (bound to bound, and bound to quasicontinuum) QWIP responsivities for samples E and F of Fig. 4. The inserts show the conduction band diagram.

wide range of high-speed long wavelength (λ = 8–12 μm) detector applications.

Detectivity

The detectivity D^* of the QWIP (i.e. the sensitivity of detecting incident radiation), depends on both the responsivity R and the total current noise i_n and is given by (6)

$$D^* = R(A\,\Delta f)^{1/2}/i_n \tag{3}$$

where A is the QWIP area. The detectivity is plotted as a function of temperature, T, in Fig. 12. for a QWIP having a long wavelength cutoff (i.e. a half sensitivity wavelength) of λ_c = 10.7 μm. Note the rapid increase of D^* with decrease in T (due to the strong decrease in i_n), with D^* rising from D^* = 10^{10} cm Hz$^{1/2}$/W at 77 K to 10^{13} cm Hz$^{1/2}$/W at T = 35 K.

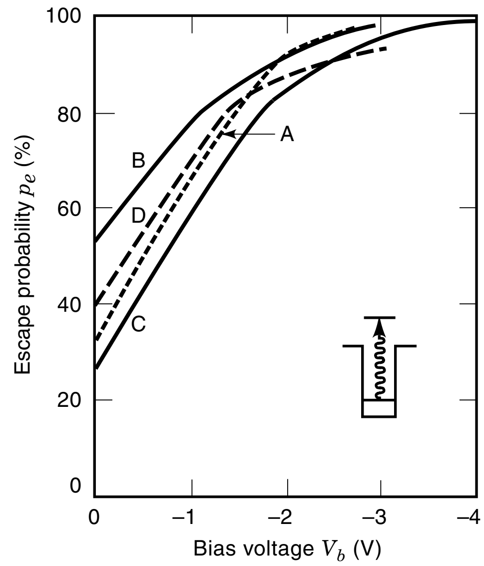

Figure 10. Escape probabilities vs. bias voltage for bound to continuum samples A–D of Fig. 4. The insert shows the conduction band diagram.

From Eq. (2), we see that if $I_d < I_p$, then the noise and hence D^* will be limited by the background photocurrent. For some applications this is a desirable situation and is called background-limited (BLIP) detection. As we will discuss later a value of $D^* \geq 10^{10}$ cm Hz$^{1/2}$/W is what is needed for excellent infrared imaging, and thus these values are more than sufficient for this purpose.

Infrared Imaging

For imaging applications (2), the most relevant figure of merit is the noise equivalent temperature difference (3,6), $NE\Delta T \propto 1/D^*$ which is the minimum detectable temperature differ-

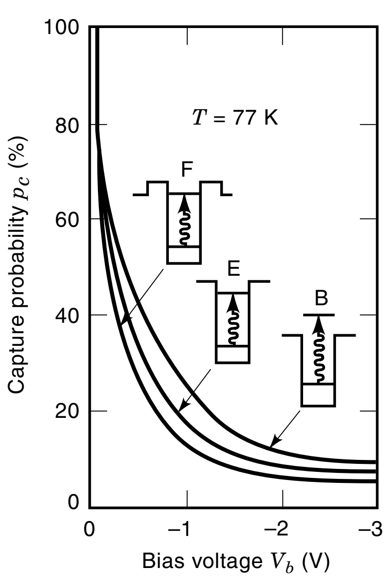

Figure 9. Quantum well capture probability vs. bias voltage for bound, continuum, and quasicontuum QWIPs. The inserts show the conduction band diagram.

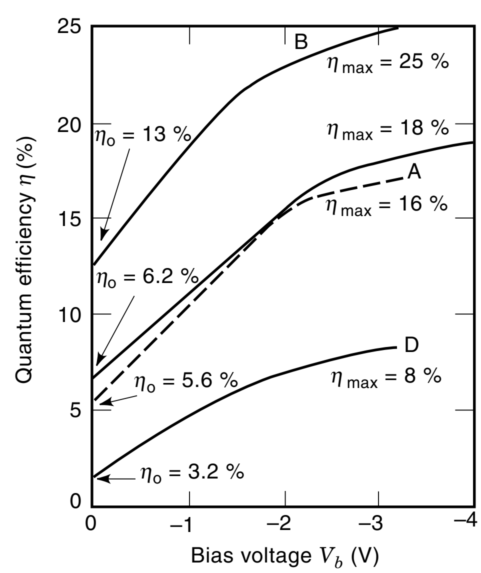

Figure 11. Quantum efficiency and escape probability vs. bias voltage for samples A–D. The insert shows the conduction band diagram.

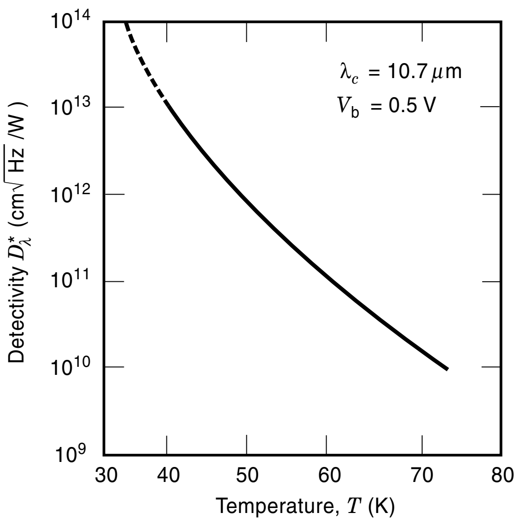

Figure 12. Detectivity vs. temperature for a bound to continuum QWIP having a cutoff wavelength of λ = 8.4 μm.

ence in an image. For optimum sensitivity in an imager with perfect pixel uniformity it is desirable for D^* and $NE\Delta T$ to be BLIP. However, for real imaging arrays the pixel nonuniformity dominates the image noise (i.e. spatial noise limited) and thus BLIP detection is *not* essential (3). This can be seen in Fig. 13, where $NE\Delta T$ is plotted against D^* with the nonuniformity u as a parameter. Note that as D^* increases, $NE\Delta T$ decreases, i.e. the imaging array becomes more sensitive. For a pixel nonuniformity of $u = 10^{-3}$ (i.e. for a nonuniformity of 0.1%), $NE\Delta T$ saturates at 60 mK for $D^* > 10^{10}$ cm $\text{Hz}^{1/2}$/W. For higher nonuniformity $u = 10^{-4}$, $NE\Delta T$ improves to 10 mK for $D^* > 10^{10}$ cm $\text{Hz}^{1/2}$/W. Thus, higher D^* is not useful when the sensitivity is limited by nonuniformity, and in this spatial noise limit, higher uniformity leads to higher performance. This is one of the main reasons that QWIPs outperform

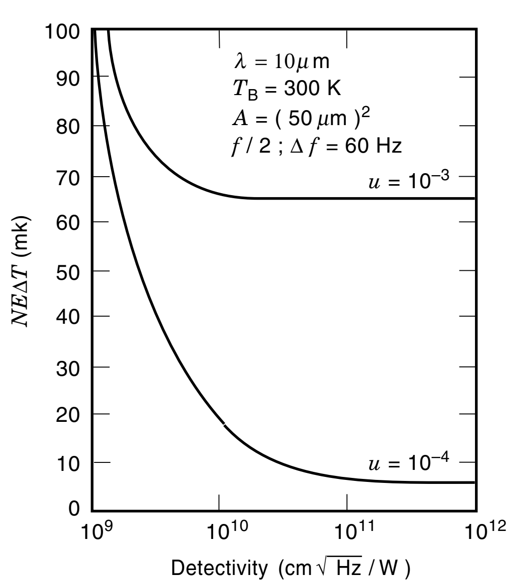

Figure 13. Noise equivalent temperature difference as a function of detectivity. The effects of nonuniformity are included for $u = 10^{-3}$ and 10^{-4}.

HgCdTe imaging arrays, since such low gap materials are very nonuniform due to difficulties in controlling the growth and processing. These nonuniformity problems get worse at longer wavelengths ($\lambda > 12$ μm) for HgCdTe since the bandgap gets even smaller. In contrast, for QWIPs the semiconductors used (GaAs, AlGaAs, InP, etc.) have large gaps and are easy to grow and process into large uniform arrays. In fact large QWIP imaging arrays (128 × 128) having λ = 15 μm have already demonstrated excellent performance (12).

Even larger GaAs/$Al_xGa_{1-x}As$ QWIP imaging arrays of 128 × 128, 256 × 256, and 640 × 484 pixels have been successfully demonstrated (13,14), at λ = 8–10 μm (Fig. 14 shows an image of a face with the 640 × 484 array). These array sizes are much larger than is possible with HgCdTe, and QWIP imagers have achieved impressive sensitivities of $NE\Delta T$ = 15 mK. These large array sizes avoid potential thermal expansion mismatch problems between the GaAs QWIPs and the Si signal processing multiplexer to which it is bonded, by thinning the QWIP array. This thinning also advantageously eliminates any optical crosstalk between pixels, although nonpixel imaging has also been proposed (15). This reduction in crosstalk is another advantage of QWIPs since it eliminates *blooming* (i.e. the saturation of weakly illuminated pixels which are near strongly illuminated pixels). Figure 14 dramatically illustrates the sensitivity and high spatial resolution of a 640 × 484 QWIP imager (14). Note, in particular, the dark cool areas on the forehead and palm which were touched by a soda can, and the clear bright head areas. Recently, small highly portable self-contained hand-held imaging cameras have been demonstrated with a size and weight comparable to home video camcorders (13), thus dramatically increasing the usefulness of QWIP cameras.

ADVANCED TOPICS

We have discussed the operation of QWIPs based on conduction band electrons in quantum wells of GaAs with $Al_xGa_{1-x}As$ barriers. In this section we will cover QWIPs based on other materials, and QWIPs using holes in the valence band.

Valence Band Hole QWIPs

From Fig. 1 we can see that quantum wells in the valence band can also have intersubband absorption if doped with holes (6,16). An important difference between the conduction band electron QWIPs (n-QWIPs) and valence band hole QWIPs (p-QWIPs) is that the conduction band is nearly parabolic and thus the quantum selection rules (i.e. the requirement of a component of the optical electrical field along the crystal growth direction) holds to a good approximation. In contrast, the valence band is nonparabolic due to multiple band interactions and thus this selection rule is relaxed, allowing absorption for electric fields perpendicular to the crystal growth direction. This eliminates the need for gratings to couple the light and is thus advantageous. However, the complexity of the valence band also has a corresponding disadvantage, namely that the photoexcited carriers are scattered much more strongly and thus the carrier lifetime is shortened, lowering the gain and responsivity. This can be seen in Fig. 15, where the responsivity of a GaAs/$Al_xGa_{1-x}As$ p-QWIP is shown for both normal incidence as well as the

Figure 14. Images taken with a QWIP camera having 640 × 484 pixels. Illustration courtesy of JPL (14).

usual 45° geometry (6). Note that both signals are comparable, due to the relaxation of the selection rules, but also that the magnitude of the responsivity is approximately an order of magnitude smaller than that for the usual n-QWIPs. Because of this smaller value of R, the sensitivity (i.e. D^* and $NE\Delta T$) are less than conduction band QWIPs and for this reason have not been used for large-area infrared imaging arrays.

Other Materials

GaAs/Al$_x$Ga$_{1-x}$As QWIPs have received the most attention due to the maturity of this crystal system and its ease of lattice matched growth; however, a number of other materials have been successfully used (6). For example, the InGaAs/InP system has a similar conduction band discontinuity to GaAs/Al$_x$Ga$_{1-x}$As and QWIPs fabricated from it have similarly high performance at $\lambda = 8$ μm. By using the lattice matched quaternary lnGaAsP/InP the bandgap of the quantum well can be increased and thus the response peak can be shifted to longer wavelengths. Correspondingly, by increasing the barrier height using the InP lattice matched InGaAs/InAlAs system, the responsivity peak can be shifted to shorter λ. This is shown in Fig. 16 where the peak at 4.0 μm is at the important short-wave atmospheric window region. This InGaAs/

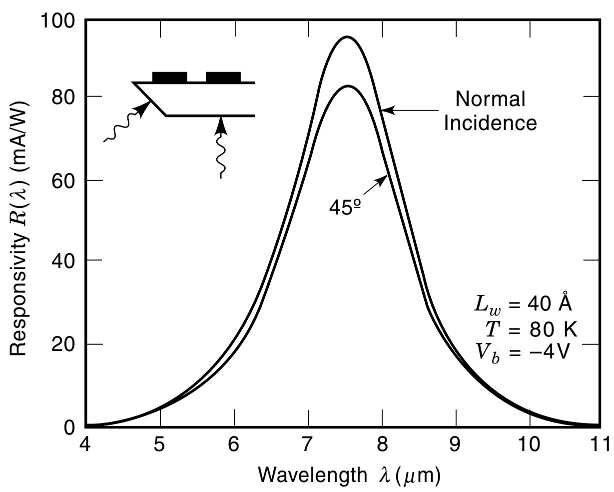

Figure 15. Comparison between the normal incidence and 45° responsivity spectra for a valence band hole QWIP.

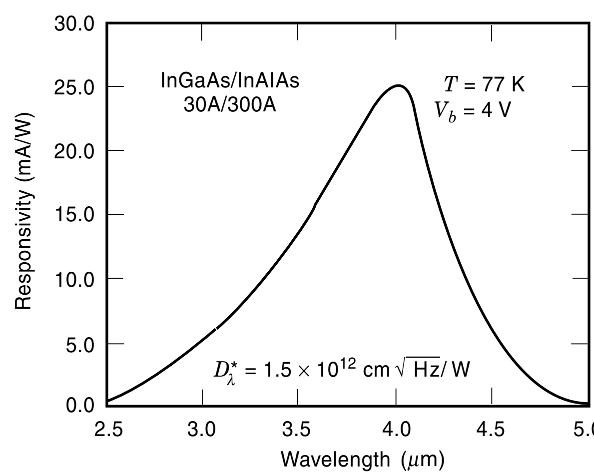

Figure 16. Responsivity spectrum for an InGaAs/InAlAs QWIP.

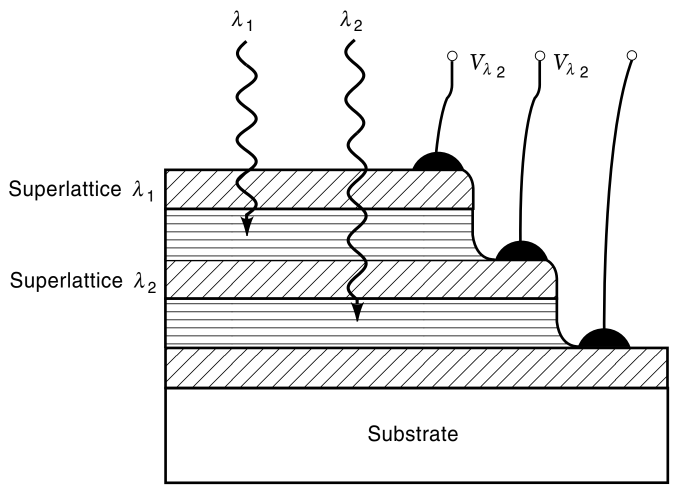

Figure 17. Schematic structure for a vertically integrated two color QWIP, allowing each wavelength to be individually addressed.

InAlAs/InGaAsP/InP system is thus particularly interesting since it can be used to span a very wide spectral range. In fact, by stacking the layers appropriately (17), (see Fig. 17) a multiwavelength QWIP (with λ from 3–20 μm) can be realized all on the same substrate. Additional QWIP materials systems which have been used include: GaAs/GaInP, GaAs/AlInP, and InGaAs/GaAs.

SUMMARY

QWIP imagers have demonstrated the highest pixel resolution (640 × 484) in the important 8–12 μm atmospheric window region, as well as achieving a very wide spectral range covering wavelengths from $\lambda < 3$ μm to $\lambda > 20$ μm. They have also achieved impressive sensitivities of $NE\Delta T = 15$ mK due to their highly uniform materials and processing technologies allowed by the use of large bandgap materials. In addition, small hand-held cameras have clearly demonstrated the practicality and low cost advantages of QWIPs over low bandgap HgCdTe, and the higher sensitivity over low quantum efficiency Schottky barrier detectors. Because of these important advantages, QWIP cameras have already been successfully used (2) in medical, firefighting, military, and night surveillance applications and are expected to find many other uses in the future.

BIBLIOGRAPHY

1. A. Sher et al., *Semicond. Sci. Technol.,* **6**: C59, 1991.
2. S. D. Gunapala et al., *SPIE,* **3061**: 292, 1997.
3. F. D. Shepard, *Infrared detectors and arrays,* SPIE, **930**: 1988.
4. B. F. Levine et al., *Appl. Phys. Lett.,* **50**: 1092, 1987.
5. L. C. West and S. J. Eglash, *Appl. Phys. Lett.,* **46**: 1156, 1985.
6. B. F. Levine, *J. Appl. Phys.,* **74**: R1, 1993.
7. J. Y. Andersson et al., *Quantum Well Intersubband Transition Physics and Devices,* H. C. Liu, B. F. Levine, and J. Y. Andersson (eds.), New York: Plenum, 1994.
8. M. Ershov, V. Ryzhii, and C. Hamaguchi, *Appl. Phys. Lett.,* **67**: 3147, 1995.
9. H. C. Liu et al., *Intersubband Transitions in Quantum Wells,* E. Rosencher, B. Vinter, and B. F. Levine (eds.), New York: Plenum, 1994.
10. W. A. Beck, *Appl. Phys. Lett.,* **63**: 3589, 1993.
11. H. C. Liu et al., *Appl. Phys. Lett.* **67**: 1594, 1995.
12. S. D. Gunapala et al., *IEEE Trans. Electron. Dev.,* **44**: 45, 1997.
13. S. D. Gunapala et al., *IEEE Trans. Electron. Dev.,* **44**: 51, 1997.
14. S. D. Gunapala et al., *SPIE,* **3061**: 722, 1997.
15. L. B. Allard et al., *Appl. Phys. Lett.,* **70**: 2784, 1997.
16. B. F. Levine et al., *Appl. Phys. Lett.,* **59**: 1864, 1991.
17. A. Köck et al., *Appl. Phys. Lett.,* **60**: 2011, 1992.

B. F. Levine
Bell Laboratories, Lucent Technologies

PHOTODIODE, AVALANCE.

See Avalanche diodes.